Materials Transactions, Vol. 43, No. 4 (2002) pp. 627 to 632
Special Issue on Radiation-Induced Effects by High Energy Particle/Solid Interaction

Influence of Ion-Irradiation on Hardness Change in Type 304 Stainless Steel Weldment Containing Delta(δ) Ferrite

Se-Hwan Chi[1], Yong-Kwan Shin[2,*], Gen-Chan Kim[1], Young-Jig Kim[3] and Jun-Hwa Hong[1]

[1]*Nuclear Materials Development Team, Korea Atomic Energy Research Institute, P.O. Box 105, Yusong, Taejon, 305-600, South Korea*
[2]*Transmission Production Team, Hyundai Power Tech., Jigokmyeon, Sosan-City, Chungnam, 356-863, South Korea*
[3]*Department of Advanced Materials Engineering, Sungkyunkwan University, Chongchon-dong, Suwon, Kyonggi-do, 400-746, South Korea*

Differences of high energy-ion induced microstructure of bcc δ-ferrite and fcc austenite matrix, and the effects of δ-ferrite on the Vickers micro-hardness (Hv) after irradiation were investigated for Type 304 stainless steel weldments containing two different δ-ferrite contents: ferrite number (FN) 5.5 and 8.5, respectively. Specimens were irradiated to 1.5 dpa with 8 MeV Fe^{+4} ions using a Tandem Vande-Graff accelerator (flux: 4.3×10^{10} ion/cm^2·s, fluence: 0.83×10^{15} ion/cm^2) at below 60°C. Calculations TRIM 95 showed that a peak damage appeared at 1.5 μm in depth with 0.7 μm full width at half maximum (FWHM). These results on irradiation-induced defects (IIDs) distribution were confirmed by TEM. Clear differences for the size and number density of IIDs as black dots (size: 5–10 nm) and loops were observed in both the austenitic matrix and δ-ferrite, where the size of IIDs was far larger in the fcc matrix than the bcc δ-ferrite. Hv test results showed that the irradiation hardening of δ-ferrite was about 1.5 times larger than the austenitic matrix. From microstructural observation the increase of the higher Vickers micro-hardness was explained.

(Received October 15, 2001; Accepted March 6, 2002)

Keywords: *irradiation effects, delta(δ) ferrite, austenitic stainless steels, dislocation loops, ferrite number, accelerator irradiation*

1. Introduction

Currently, the ferrite content in the weld filler metal is required to be depicted by a ferrite number (FN) between 5 and 20 in relation to the residual delta(δ)-ferrite in the austenitic stainless steel weldment after the welding of austenitic stainless steel core support structures and Class 1 and 2 components in Section III, ASME boiler and pressure vessel code. The lower limit provides sufficient ferrite to avoid microfissuring in the weld, whereas the upper limit of residual delta(δ)-ferrite provides a ferrite content adequate to offset dilution.[1)] Thus, the upper limit is to minimise embrittlement of the weld in service and the lower one to prevent solidification cracking of the weld during the component fabrication.

Contrary to these beneficial effects of the ASME code specified delta(δ)-ferrite content in the austenitic stainless steel weld, some detrimental effects are expected to occur due to the difference in the crystal structure between the body-centered cubic (bcc) delta(δ)-ferrite and face-centered cubic (fcc) austenite matrix. Especially significant differences in the radiation sensitivity of the fcc and bcc crystal have been observed by computer simulation or experimental studies under irradiation conditions.[2–6)] In this sense, the integrity of the weld is very important to the nuclear components made of stainless steel, and it is necessary to characterize the radiation sensitivity of the delta(δ)-ferrite compared with the fcc austenite matrix in the stainless steel welds under irradiation conditions as an input for the safety and lifetime evaluation of the welded stainless steel reactor component.

In the present study, using two nuclear grade austenitic stainless steel welds with different delta(δ)-ferrite content, the influence of delta(δ) ferrite on irradiation effects in type 304 stainless steel weld was characterized by the investigation of the differences in the irradiation-induced defect microstructure of bcc delta(δ)-ferrite and fcc austenitic stainless steel weld matrix, and by identifying the contribution of bcc delta(δ)-ferrite to the irradiation-induced increase in the Vickers microhardness of the weld.

2. Experimental

2.1 Material and specimen

Two weld coupons with ferrite number (FN) 5.5 and 8.5, were prepared from two filler metals, 308L or 308L plus 309L, and two different welding methods: submerged arc welding (SMAC) or flux cored arc welding (FCAC). Details of welding processes are reported elsewhere.[7)]

Since a diluted weld deposit shows a range of FN depending on the specific direction and location, great attention was given before and after machining specimens (10 mm × 1.3 mm × 0.5 mm) from the coupons to identify and group the specimens by FN using a Ferrite Content Meter (model 1.054).

All of the specimen surfaces for ion-irradiation and Vickers microhardness measurement were mechanically polished (up to 0.3 μm Al_2O_3) followed by electropolishing for two minutes (at room temperature) at a current density of 0.15–0.2 A/cm^2 using a solution made of acetic acid (95 mL) and perchloric acid (5 mL).

Chemical compositions of the type 304 stainless steel plate and filler metals used are shown in Tables 1–3. Figure 1

*Former Graduate Student, Department of Advanced Materials Engineering, Sungkyunkwan University, Chongchon-dong, Suwon, Kyonggi-do, 400-746, South Korea.

Table 1 Chemical composition of Type 304 stainless steel (base metal) (mass%).

C	Ni	Cr	Mn	P	S	Si	N	Fe
0.045	8.66	18.1	1.06	0.027	0.002	0.56	0.05	Bal.

Table 2 Chemical composition of the filler metal for FN 8.5 weld (mass%).

C	Si	Mn	P	S	Ni	Cr	Cu	Mo	V	Cb + Ta	N	Ti	Fe
0.025	0.78	0.97	0.022	0.003	9.54	19.5	0.12	0.08	0.08	0.011	0.064	0.019	Bal.

Table 3 Chemical composition of the filler metal for FN 5.5 weld (mass%).

C	Si	Mn	P	S	Ni	Cr	Co	Cu	Mo	V	Cb + Ta	N	Ti	Fe
0.047	0.698	1.146	0.023	0.003	10.72	20.66	0.09	0.15	0.12	0.07	0.001	0.056	0.02	Bal.

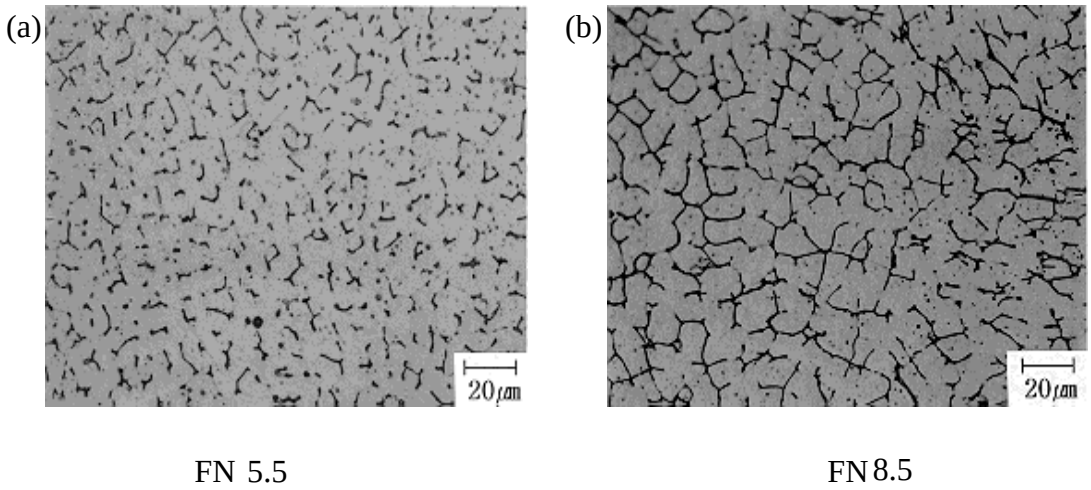

Fig. 1 As-received optical microstructure of (a) FN 5.5 and (b) FN 8.5 Type 304 stainless steel weldment.

shows optical micrographs of the weldments having two different FN numbers: FN 5.5 and FN 8.5. The microstructure of the weld was two-phase, *i.e.* austenitic and delta(δ)-ferritic.

2.2 Irradiation and TRIM calculation

Irradiation of specimens was performed by 8 MeV Fe^{+4} ions to 1.5 dpa using a Tandem Vande-Graaff accelerator (model: NEC 5SDH-2) in KIGAM (Korea Institute of Geology and Mining). It has been reported that the largest irradiation-induced change in yield strength of austenitic stainless steel is obtained at 1.5 dpa at the irradiation temperature of 60°C.[8,9] Therefore, the target dose 1.5 dpa was chosen to induce a maximum yield strength change after irradiation. The beam current was 250 nA (flux: 4.3×10^{14} ions·m^{-2}·S^{-1}, fluence: 0.83×10^{19} ions·m^{-2}), and the irradiation period was 20,000 s. TRIM95 was used to determine the irradiation dose and accelerator condition with 40 eV Fe atom displacement energy. The beam diameter was 5 mm. The irradiation chamber was kept in a vacuum of 10^{-6} Torr and the irradiation temperature was not over 60°C.

2.3 Microstructure examinations

Optical, scanning electron microscopy (SEM) and transmission electron microscopy (TEM) were used to observe delta(δ)-ferrite microstructure (size and morphology), and irradiation-induced defect microstructure and for diffraction analyses. For optical microscopy, specimen surface was etched using a solution made of $HCl : HNO_3 : H_2O = 5 : 1 : 7$ for 10 s.

TEM observations of irradiation-induced defects microstructure at a range ($\sim 1.5\,\mu m$) were performed by means of a cross section method after plating a thin iron layer followed by a thick nickel plate on the irradiated specimen.[10,11] A thin layer of Fe plating ($< 0.2\,\mu m$) was necessary to improve the adhesion of Ni plating onto the irradiated specimen surface.[12]

Schematics of a cross-sectional TEM specimen preparation and the details of Fe and Ni plating procedure are shown in Fig. 2 and Table 4,[13] respectively. Thinning was done by ion milling with 4.5 keV Ar ions.

2.4 Microhardness measurement

To evaluate the influence of delta(δ)-ferrite on the irradiation hardening in the weld, Vickers microhardness (Hv) tests were conducted. A test load of 0.05 N (~ 5 g) was determined by considering indenter penetration depth against a range. Since the indenter size (diagonal) of 0.05 N load ($\sim 7\,\mu m$) was larger than the size of delta(δ)-ferrite ($\sim 1\,\mu m$

Table 4 Fe and Ni plating procedure and condition.

(a) Fe plating		
Pre-treatment	(1) Copper wire spot welding on the unirradiated surface: < 10 mV (2) Cleaning: ultrasonic cleaning in acetone. Then, methanol cleaning (3) Surface activation treatment: 10–30 s in 5% citric acid (40–50°C)	
Ferrous chloride bath	(1) Solution 1: $FeCl_2$ 225 g + pure water100 mL (2) Solution 2: $CaCl_2$ 250 g + pure water 125 mL (3) Addition of 3 g active charcoal in mixed solution (1) and (2) (4) Heating 1 h, and filtering 2–4 times (5) Make 1 L bath with pure water addition. Fe-plating	
Fe-plating	(1) Current density: 800–1,500 A/m^2 (2) Plating rate: ~ 50 μm/h	
Ferrous chloride bath concentration and pH control (0.8–1.5)	(1) Keep ferrous chloride concentration > 1000 ppm with high purity iron powder (< 1 g) and 5% hydrochloric acid (2) Add 5% hydrochloric acid if pH > 1.5 (3) Add ferrous carbonate or ferrous hydroxide if pH < 0.8	
(b) Ni plating		
Ni-plating solution	(1) Solution: $NiSO_4$(260 g) + $NiCl_2$(45 g) + H_3BO_3(45 g) + Udylite#63 10 mL	
Ni-plating condition	(1) Temperature: 40–50°C	(2) Current density: 200–600 A/m^2 (4) Plating rate: ~ 0.7 μm/h
	(3) pH: 4.0–4.8	

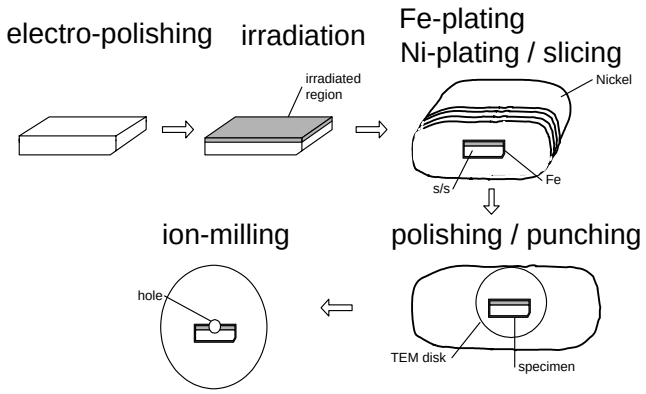

Fig. 2 Schematic of a cross-sectional TEM specimen preparation procedure.

in width) (Fig. 1), it was impossible to measure the Vickers microhardness of delta(δ)-ferrite before and after irradiation without the influence of a matrix. For this reason, under the assumption of a Gaussian distribution of Hv for a phase, Hv-probability curves were obtained through 120 and 70 Hv measurements before and after irradiation for a matrix with or without delta(δ)-ferrite, *i.e.* Hv($\delta + \gamma$) or Hv(γ), respectively. From the curve, the Hv of un-irradiated and irradiated delta(δ)-ferrites was determined by decomposing a two-phase Hv distribution curve Hv($\delta+\gamma$) into two Gaussian curves, one for each phase, *i.e.* Hv(δ) and Hv(γ). Detailed implementation of the method is given in Section 3.3.

Tests were conducted for 15 s loading condition at room temperature.

3. Results and Discussion

3.1 Damage depth profile and defects size distribution

Figure 3 shows the results of TRIM95 calculation for the damage depth profile and TEM microstructure in the irradiated area. It is shown that the peak damage depth (range) appears at around 1.5 μm with about 0.7 μm full with at half maximum (FWHM). The distribution of irradiation-induced defects (black dots and loops) in Fig. 3(b) shows coincidence with the TRIM95 calculation. A lot of irradiation-induced defects were observed throughout the matrix parallel to the ion incident surface forming a thick dark band irrespective of delta(δ)-ferrite content. The average size of the defects in the austenite weld matrix and delta(δ)-ferrite was 14.6 ± 10.2 nm and 6.4 ± 3.5 nm, respectively.

3.2 Differences in the irradiation-induced defect microstructures between the austenite matrix and delta(δ) ferrite

Figure 4 shows the defect microstructures before and after irradiation both for delta(δ)-ferrite and austenite matrix. The microstructure of delta(δ)-ferrite and austenite matrix before irradiation showed no large difference in TEM as well as optical microstructure. However, it is seen in Figs. 4(b), (d) and Fig. 5 that irradiation-induced defects (black dots, and black and white contrasts) are formed both in the delta(δ)-ferrite and austenite matrix, and the size and density in delta(δ)-ferrite are smaller and lower than austenite matrix. Thus, a large number of defects with size of 5–25 nm were found in the weld austenite matrix, while smaller defects (about 43% of the average fcc austenite weld matrix defect size) with lower density were found in delta(δ) ferrite.

These differences in the size and number density of defects between the delta(δ)-ferrite and austenite matrix may be attributed to the difference in the defect accumulation rate for

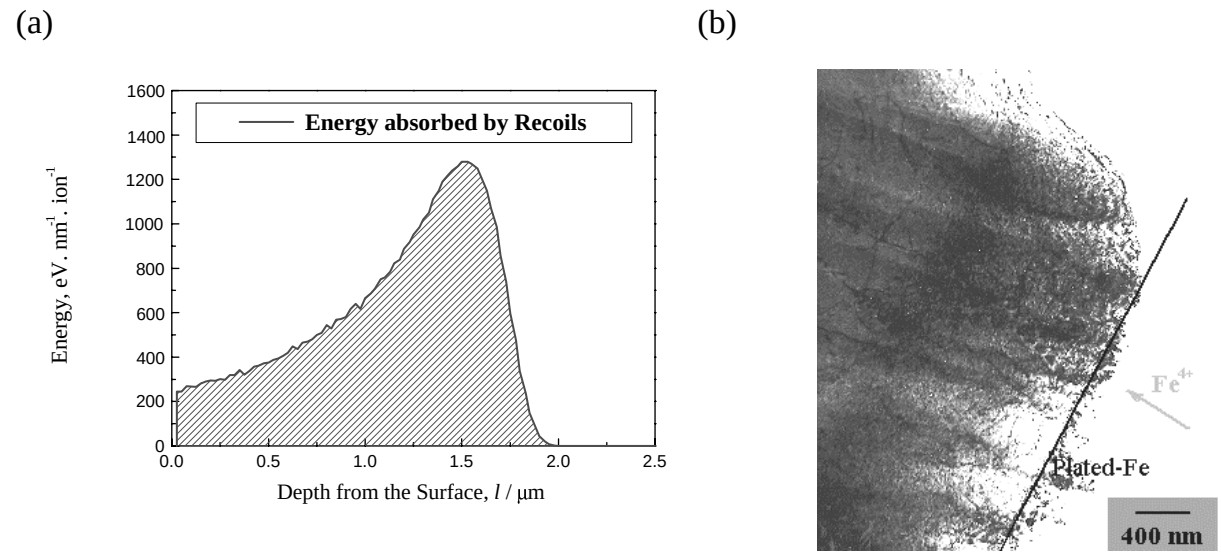

Fig. 3 (a) TRIM95 result and (b) distribution of irradiation-induced defects. Peak damage depth and FWHM are seen to be about 1.5 μm and 0.7 μm in (b), respectively.

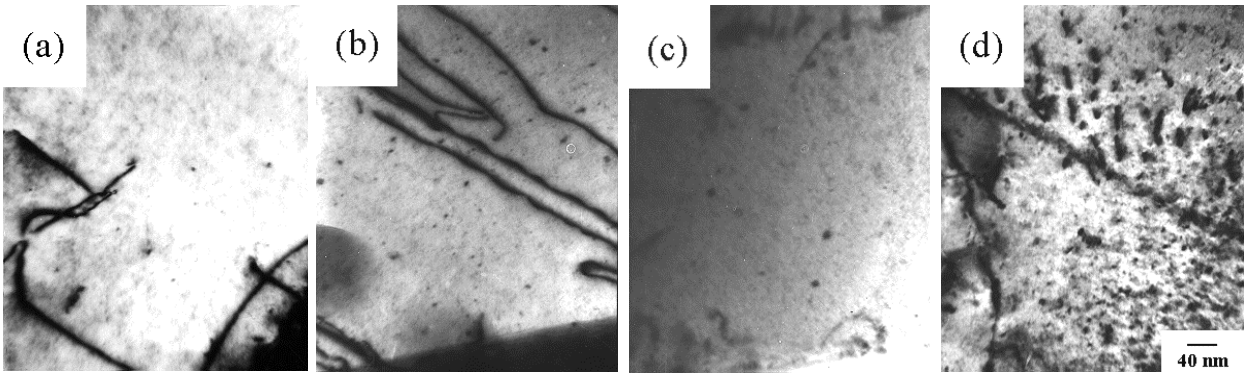

Fig. 4 TEM microstructure for as-received and irradiated δ ferrite and austenite matrix. (a) δ ferrite, 0 dpa. (b) δ ferrite, 1.5 dpa. (c) austenite matrix, 0 dpa and (d) austenite matrix, 1.5 dpa.

the fcc and bcc crystals. Victoria *et al*. suggested that higher dose is needed to obtain the same cluster density in bcc Fe than that in fcc Cu.[5] The reason for the difference in the defect accumulation rate is not clear at present. However, it is, from the computer simulations of cascade evolution, indicate that stable stacking fault tetrahedra (SFT) results from large cascades (for PKAs $\sim$30–50 keV) in Cu,[14] and interstitial loops resulting from the cascade quenching in Fe are much smaller and highly mobile.[15–17] Thus, comparing to fcc austenite matrix, it seems that little chances are available to form large size irradiation-induced defect (IID) clusters which are visible by TEM in bcc delta(δ)-ferrite.

Regarding the type of defects which is known to depend on the stacking fault energy (SFE), most of the defects of black and white contrasts in Fig. 5 was identified as dislocation loops from the perpendicular relation between $\bar{g}$ the operating reflection and the sense of the black-white contrast associated with the irradiation-induced defects under the two beam conditions.[18] Actually, the main defect clusters in the irradiated austenitic stainless steel with low SFE are known as loops, even SFTs are dominantly observed in austenitic stainless steels with low SFE.[5]

3.3 Vickers microhardness change with crystal structure after irradiation

Figure 6 shows the increase in the Vickers microhardness after irradiation for each test load from 0.05 to 10 N. The increase in the Hv due to irradiation was the largest for the 0.05 N test load irrespective of FN. The calculation of the indentation depth indicates that indentation at 0.05 N load with a possible influence of loading resides within the highly damaged region (range plus FWHM) during the test. It is seen that the higher is the FN, the larger the increase in the Hv due to irradiation. Thus, FN 8.5 weld increased 10% at 0.05 N load more than FN 5.5 in H_V after irradiation.

Figure 7 shows the change in the distribution of the Vickers microhardness in two-phase weld after irradiation. It is seen that the increase in Hv is larger in the matrix with delta(δ)-ferrite than the delta(δ)-ferrite free matrix. Thus, the former increased from about 178 to about 216, and the latter increased from about 168 to 193. From these results, it is obvious that the irradiation sensitivity of delta(δ)-ferrite is higher than the fcc matrix.

To estimate and compare in more detail the irradiation sensitivity for the fcc matrix and bcc delta(δ)-ferrite, we tried to decompose the unirradiated matrix (two-phase) Hv distribution curve, Hv($\delta + \gamma$), into two Hv Gaussian curves, *i.e.*, fcc

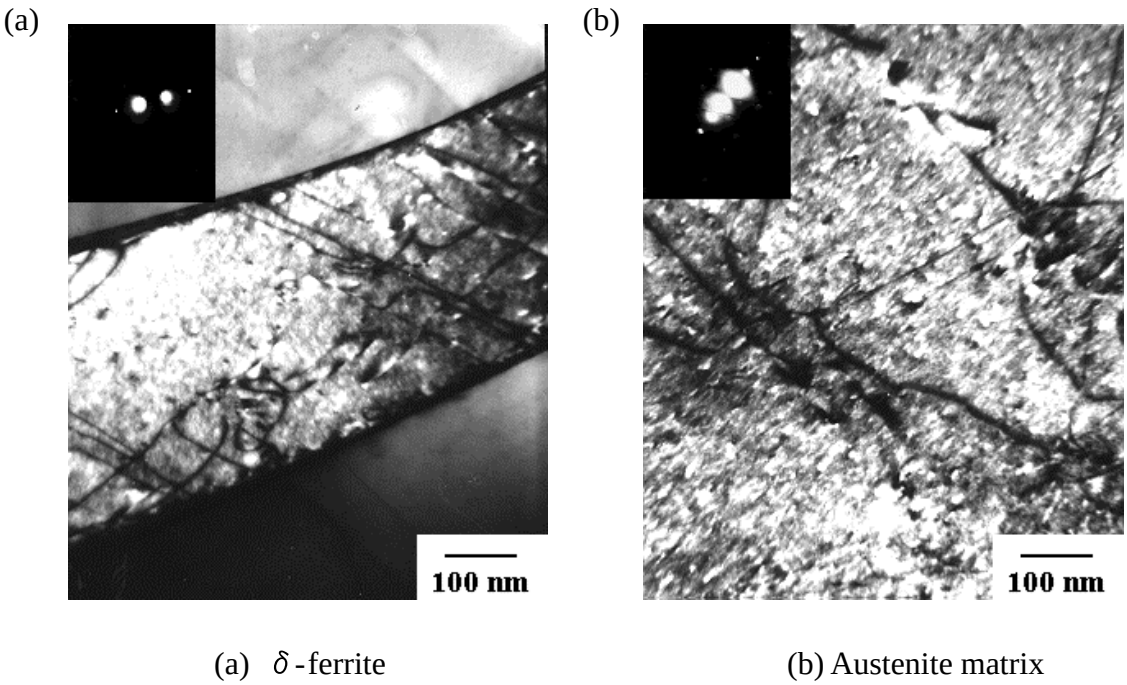

Fig. 5 Defects analysis under two beam condition. It is seen that most of the lines of contrast are perpendicular to $\bar{g}$, the operating reflection. (a) bcc $[\bar{1}11]$ zone, $\bar{g} = [0\bar{1}1]$. (b) fcc $[\bar{1}12]$ zone, $\bar{g} = [1\bar{1}1]$.

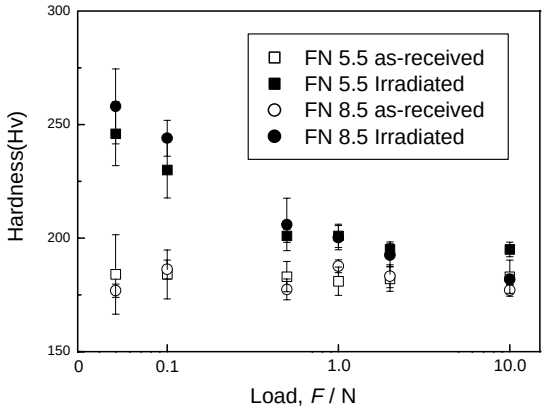

Fig. 6 Test load (0.05–10 N) effects on the irradiation-induced Vickers microhardness in the as-received and irradiated FN 5.5 and 8.5 welds.

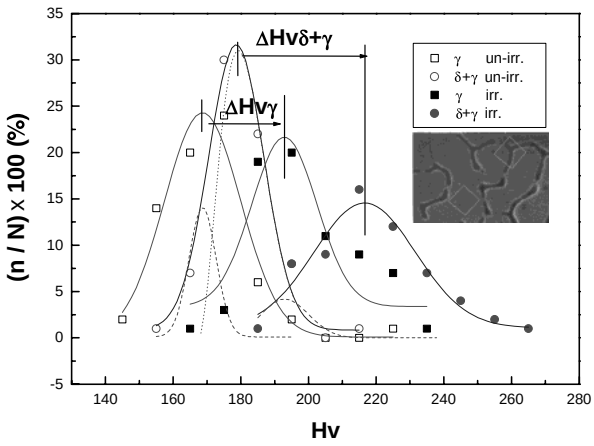

Fig. 7 Determination of phase contribution to the Vickers microhardness increase after irradiation. The average δ-ferrite area measured by an image analyser for 120 and 70 indentations before and after irradiation, respectively, was about 25% of the 0.05 N load indentations.

matrix (dash line) and bcc delta(δ)-ferrite (dot line) as shown in Fig. 7, by assuming the maximum Hv(γ) of a matrix without delta(δ)-ferrite and also assuming that the decomposed Hv(γ) curve from the two-phase Hv($\delta + \gamma$) are the same and the decomposed Hv(γ) curve (dash line) is contained in the two-phase Hv($\delta+\gamma$) curve. Thus, the Hv(δ) distribution curve (dot line) was obtained by subtracting the Hv(γ) curve (dash line) from the two-phase Hv($\delta + \gamma$) curve.

The same assumption and decomposition method were applied to the irradiated matrix Hv distribution curve. From the analysis it is clarified that the Hv of two-phase matrix is the same value for the Hv of delta(δ)-ferrite in both the unirradiated and irradiated matrixes.

This analysis showed that the delta(δ)-ferrite may be assumed to be hardened from 178 to 216. This result indicates that the delta(δ)-ferrite became harder by 1.5 times more than the fcc matrix.

The higher hardening behavior in bcc delta(δ)-ferrite than fcc austenite matrix may be understood by the difference in the irradiation-induced defects microstructure, but not restricted to the defect number density. Recent studies on the difference due to crystal structure suggest that there are differences in the defect cluster size distribution, defect accumulation behavior, the migration mechanism of self-interstitial atom (SIA), the fraction of glissile SIA clusters produced in the cascades, and the interaction of dislocation with glissile defect clusters.[4] The invisible irradiation-induced defects in the bcc delta(δ)-ferrite (in Fig. 4(b) and Fig. 5(a)) by TEM seem to be a characteristic of bcc crystal for its higher hardening behavior than the fcc austenite matrix. Higher defect accumulation and growth rate in the fcc matrix will occur visible larger size defects visible by TEM than bcc delta(δ)-ferrite resulting in a fast decrease in the number density of

small defects which are effective in friction hardening. Thus, to compare the bcc delta(δ)-ferrite of fine and invisible, but larger in number density defects to the fcc matrix of fewer but larger defects, will show a higher sensitivity to irradiation hardening.

Currently, in the bcc reactor pressure vessel steels, invisible defects by TEM with fine size ($\sim < 5$ nm) are characterized by SANS and AP/FIM.[19)]

4. Conclusion

From the Vickers microhardness measurements on 8 MeV Fe^{+4} ion irradiated (1.5 dpa) delta(δ)-ferrite containing austenite weld, the irradiation sensitivity of bcc delta(δ)-ferrite appeared to hardened about 1.5 times more than fcc austenite matrix possibly due to its fine defect rarely visible by TEM. A higher defect growth rate in the fcc weld matrix to bcc delta(δ)-ferrite was confirmed. The average defect size in fcc austenite matrix was about 2.3 times larger than those of bcc delta(δ)-ferrite, *i.e.*, 14.6 nm versus 6.4 nm. From the perpendicular relationship between $\bar{g}$ the operating reflection and the sense of black and white contrast, most irradiation-induced defects were analyzed to be dislocation loops irrespective of crystal structure.

Acknowledgements

The authors wish to express their sincere gratitude to Mr. J. H. Baik, general manager, quality assurance dept., DooSan Heavy Industry (Former Korea Heavy Industries and Construction Co., LTD), for supplying the nuclear grade weld coupons, Mr. Y. Y. Kim, KINS, for the ferrite content meter, Mr. H. D. Cho and Dr. Y. S. Im, KAERI, for TEM microscopy and defects analysis, respectively, and Dr. H. W. Choi, KIGAM, for ion irradiation by KIGAM Tandem accelerator. This work has been carried out as a part of the Reactor Pressure Boundary Materials Project under the Nuclear R&D Program by MOST, Korea.

REFERENCES

1) U. S. Nuclear Regulatory Commission Regulatory Guide 1.31, Control of Ferrite Content in Stainless Steel Weld Metal, Revision 3, April, 1978.
2) B. N. Singh and J. H. Evans: J. Nucl. Mater. **226** (1995) 277–285.
3) M. Kiritani: J. Nucl. Mater. **276** (2000) 41–49.
4) A. Almazouzi, T. Diaz de la Rubia, B. N. Singh and M. Victoria: J. Nucl. Mater. **276** (2000) 295–296.
5) M. Victoria, N. Baluc, C. Bailat, Y. Dai, M. I. Luppo, R. Schaublin and B. N. Singh: J. Nucl. Mater. **276** (2000) 114–122.
6) A. Iwase and S. Ishino: J. Nucl. Mater. **276** (2000) 178–185.
7) Unpublished Certified Material Test Report, KHIC, 1998.
8) E. E. Bloom, W. R. Martin, J. O. Stiegler and J. R. Weir: J. Nucl. Mater. **22** (1967) 68–76.
9) K. Shiba, T. Sawai, S. Jitsukawa, A. Hishinuma and J. E. Pawel, J.: *Effects of Radiation on Materials*: 17th Int. Symp., ASTM STP 1270, David S. Gelles, Randy K. Nanstad, Arvind S. Kumar and Edward A. Little, Eds., (ASTM, 1996) pp. 971–979.
10) G. A. DiBari: Metal Finishing, **98** (2000) 270–288.
11) C. F. Lowrie: Metal Finishing, **98** (2000) 266–269.
12) A. Kimura, H. Shibamoto, H. Yuya, S. Yamaguchi and H. Matsui: *Effects of Radiation on Materials*: 17th Int. Symp. ASTM STP 1270, David S. Gelles, Randy K. Nanstad, Arvind S. Kumar and Edward A. Little, Eds., (ASTM, 1996) pp. 220–231.
13) Yong-Kwan Shin: *A Study on the Influence of δ-Ferrite on the Irradiation Effects in Type 304 Stainless Steel Weldment*, Master Thesis, SungKyunKwan University, 2000.
14) K. Nordlung and F. Gao: Appl. Phys. Lett., submitted.
15) W. Phythian, R. E. Stoller, A. J. E. Foreman, A. F. Calder and D. J. Bacon: J. Nucl. Mater. **223** (1995) 245–261.
16) M. J. Caturla, N. Soneda, E. Alonso, B. Wirth, T. Diaz de la Rubia and J. M. Perlado: J. Nucl. Mater. **276** (2000) 13.
17) Y. N. Osetsky, D. J. Bacon, A. Serra, B. N. Singh and S. I. Goolubov: J. Nucl. Mater. **276** (2000) 65–77.
18) M. H. Loretto and R. I. Smallman: *Defect Analysis in Electron Microscopy*, (Chapman and Hall, London, 1975) pp. 77–88.
19) G. R. Odette and G. E. Lucas: *Proc. of Ishino Conference*, (The University of Tokyo, 1994) p. 30.